Prioritized Coordinated Reactive Power Control of Wind Turbin Involving STATCOM Using Multi-Objective Optimization

Amir Moghadasi, *Student Member, IEEE,* Masood Moghaddami, *Student Member, IEEE,* Arash Anzalchi, *Student Member, IEEE,* Arif Sarwat, *Member, IEEE,* and Osama A. Mohammed, *Fellow, IEEE*

***Abstract*—This paper presents a computational intelligence technique for optimal coordinated reactive power control between a wind turbine (WT) equipped with doubly fed induction generator (DFIG) and a static synchronous compensator (STATCOM), during faults. The proposed control model is formulated as a multi-objective optimization problem (MOP) in order to simultaneously minimize two conflicting objectives: 1) voltage deviations at the WT terminal during and after grid faults and 2) low-frequency oscillations of the active power after clearing the faults. For this purpose, it is necessary to achieve the optimal values of control variables, such as the reactive power references for both DFIG and STATCOM controllers. The aforementioned problem is solved by using the stochastic normalized simulated annealing (NSA) algorithm. Since the proposed problem is a MOP incorporating several solutions, the NSA algorithm finds the Pareto-optimal solutions for the proposed control system, based on the assigned priorities (weights) for each objective. For online applications, where the control system needs to act very fast, a fuzzy logic controller (FLC) is used, so that tuning the fuzzy model and fuzzy rules are accomplished offline by the NSA algorithm. To validate the effectiveness of the proposed control strategy, a case study including a 1.5-MW DFIG and a 1.5-MVar STATCOM were carried out with MATLAB/Simulink.**

***Index Terms*—Fuzzy logic controller, multi-objective optimization, optimal reactive power control, pareto optimality, simulated annealing (SA), STATCOM.**

I. Introduction

THE majority of wind turbines (WTs) in power systems are equipped with doubly fed induction generators (DFIGs) [1]-[4]. This technology offers the advantages of the variable speed operation with active and reactive powers control using both the rotor-side converter (RSC) and grid-side converter (GSC), which are rated for only a small fraction ($25\% \sim 30\%$) of the rated power generators. Since many WTs have been electrically integrated into a weak power grid, the DFIG converters are not able to provide adequate reactive power and voltage support, due to their limited capacity, and thus, there can be a risk of voltage collapse [1]. On the other hand, a sudden lack of the active power generation, due to providing the reactive power with the DFIG during the fault, might cause power unbalance in the system, which results in low-frequency oscillations of the active power after clearing the fault, and thereby increasing the risk of frequency instability [4]. The applications of the static synchronous compensators (STATCOMs), which are commercially available and practically installed in the power system, are being increasingly proposed to provide a rapid and controllable reactive power compensation, helping with the uninterrupted operation of WTs under disturbances [1], [4], [5]. However, a DFIG has a complicated structure including several components, and the inclusion of a STATCOM makes this layout more problematic for the optimal and real-time control of the power system.

The stability analysis and optimal control of the DFIG-based WTs have been studied by many researchers using optimization-based approaches [2], [6]-[11]. In [6], the bacterial foraging algorithm (BFA) is used for the optimal control of a DFIG system. Authors in [7] described a new modified model of the genetic algorithm (GA) for optimal control design of a large offshore wind farm. The particle swarm optimization (PSO) algorithm was proposed for the DFIG-based WT systems to find optimal values of both converter and active damping controllers [2], [8]. An optimal coordination of the DFIG converters through a fuzzy controller, which is designed using the GA was proposed in [9] to enhance the LVRT capability of WTs. Other advanced coordinated control approaches, such as adaptive dynamic programming (ADP) based methods have shown promising results for such a challenging problem [10], [11]. Also, the application of a STATCOM to improve the capability of a wind farm (equipped with DFIGs) to ride through grid faults in a multi-machine power system has been reported in [1]. However in [1], there is no coordination between the wind farm and the STATCOM for the reactive power control. In [4], authors proposed a heuristic dynamic programming (HDP) based on the coordinated reactive power control of a large wind farm and a STATCOM to reduce the level of the voltage dip during the fault and improve the post-fault power oscillation damping of the system. Although these optimization-based techniques have shown promising results for the proper optimal operation of the system, there are some deficiencies, mainly addressing single-objective optimization problem.

In a multi-objective optimization problem (MOP), since several objectives of the system can be simultaneously optimized based on their priority; Pareto-optimal solutions can be obtained instead of a single optimal solution, which represents the best possible trade-off between the objectives [12], [13]. A decision maker can select any of the Pareto-optimal solutions based on his/her own preference. A breakthrough in obtaining Pareto solutions has been realized by the application of stochastic methodologies, such as GA, PSO, and normalized simulated annealing (NSA) algorithm [14]. Among these algorithms, NSA has the major advantage to avoid becoming trapped at a local minima [12], [14].

The key motivation of this study is to design a coordinated reactive power controller that is formulated as a MOP model. By decreasing the level of the voltage deviations at the WT

978-1-4673-8672-2/15/$31.00 © 2016 IEEE

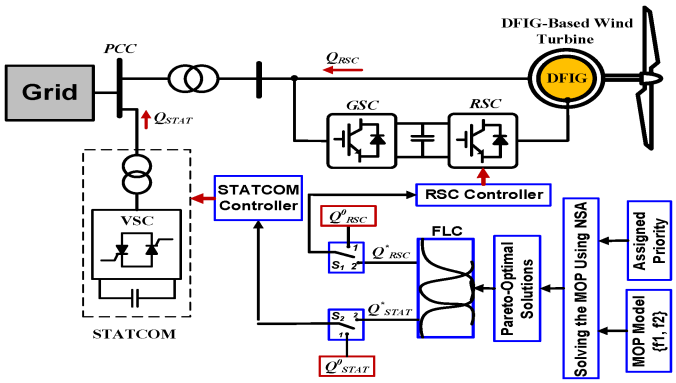

Fig. 1. Overall block diagram of the proposed PCRPC for online application.

terminal, the low voltage ride-through (LVRT) capability of the WT can be significantly improved. Thus, one objective function considered in this paper is the voltage deviations. This paper also proposes an index called transient power severity index (TPSI) to quantify the transient active power performance of the system after the fault clearing time. The minimization of the TPSI for system buses is considered as the second objective function. In order to minimize these two objective functions, it is necessary to find the optimal value of control variables, which are the reactive power references for both DFIG and STATCOM controllers. For the online coordinated reactive power control, the obtained optimal signals of the reactive power references are used in a fuzzy logic controller (FLC) for offline tuning the fuzzy model and fuzzy rules.

The main contributions and novelties of the proposed approach are as follows: 1) the proposed coordinated reactive power control is formulated as a MOP model to minimize the voltage deviations at the WT terminal during and after the faults and TPSI after clearing the faults; 2) the NSA algorithm is employed to find pareto-optimal solutions of the MOP model. Compared to the GA method, it is clearly confirmed the NSA exhibits considerably lower computational times; 3) the FCL is properly tuned by the NSA algorithm for the online application; 4) the performance of the proposed control approach is successfully validated with simulation results.

II. Coordinated Reactive Power Control

In this section, a multi-objective optimization problem (MOP) model, a stochastic normalized simulated annealing (NSA) algorithm, and a fuzzy logic controller (FLC) are used to design an external interface controller for the coordinated reactive power control between the DFIG and the STATCOM, as shown in Fig. 1. A DFIG-based WT technology is used in this paper, because the majority of WTs in power systems are equipped with DFIGs, and a STATCOM is also employed due to its superior dynamic characteristics. However, the proposed coordinated control method is applicable for other similar devices, such as a permanent magnet synchronous generator (PMSG)-based WT and static VAR compensator (SVC).

The MOP model is first formulated in order to simultaneously minimize two conflicting objectives: 1) voltage deviations at the point of common coupling (PCC) during and even after the grid faults and 2) low-frequency oscillations of the active power after clearing the faults. In this paper, the control variables of the proposed MOP are the reactive power references of Q^*_{RSC} and Q^*_{STAT} for both RSC of the DFIG and STATCOM controllers, respectively. The proposed MOP model is then solved by the NSA algorithm in order to find the Pareto-optimal solutions, based on the assigned priorities (weights) for each objective. Each of the Pareto-optimal solutions is used for offline tuning the fuzzy model and fuzzy rules of the FLC. The reason for selecting a NSA-based approach for tuning the FLC is that the derivation of rules from the simple fuzzy reasoning is totally complicated due to the complexity and nonlinearity of the power network. For online applications, the main use of the FLC is that it can quickly change the Q^*_{RSC} and Q^*_{STAT} during grid faults, it is possible to reduce the level of voltage reductions at the PCC, and to rapidly dampen the low-frequency oscillations of the active power in the system.

The overall block diagram of the proposed control approach is shown in Fig. 1. In this paper, no effort will made to optimize the steady-state control system, as the goal of the paper emphasizes only the encounter of the faults. Thus, switches S_1 and S_2 are kept in position 1 in the steady-state condition with fixed reactive power commands of the Q^0_{RSC} and Q^0_{STAT}. Once the fault occurs, S_1 and S_2 switch to position 2 and the FLC, as an external online controller, provides the coordinated reactive power control for the STATCOM and the RSC.

A. MOP Model Formulation

In this section, the proposed coordinated reactive power control is formulated as a multi-objective programming model with the following objectives and constraints.

1) Objectives: When a fault occurs at some points of the grid, the WT experiences a voltage sag situation at the PCC and may disconnect from the grid due to a severe voltage stability issue. This problem can be solved by supporting the reactive power during the fault in order to decrease the level of voltage reductions, and thereby improve the fault ride-through capability of the WT. In this effort, the voltage severity index (VSI) is defined to quantify the deviation of the voltage at the PCC, given by

$$\text{VSI} = \frac{\sum_{t=T_s}^{T} \Delta V^t_{PCC}}{T - T_s} \tag{1}$$

where T is the considered transient time frame, T_s is the fault starting time, and ΔV_{PCC} is the voltage deviation, calculated by

$$\Delta V^t_{PCC} = \begin{cases} \frac{|V^t_{PCC} - V^0_{PCC}|}{V^0_{PCC}}, & \text{if} \quad \frac{|V^t_{PCC} - V^0_{PCC}|}{V^0_{PCC}} \geq \alpha \\ 0, & \text{otherwise} \end{cases} \tag{2}$$

where V^0_{PCC} is voltage magnitude at the PCC before the fault occurrence, V^t_{PCC} is the voltage magnitude of the PCC at time t obtained from time-domain simulation, and α is the threshold to define unacceptable voltage deviation level, which can be set according to the international grid codes, e.g., 10% for Danish grid codes [15].

Also, the sudden lack of the active power generation, due to providing the reactive power with the RSC of the DFIG,

might cause a power imbalance during the fault. This will excite the low-frequency oscillations on the generator rotor angle, resulting in fluctuations of the active power. This paper proposes a transient power severity index (TPSI) to quantify the transient power performance of the system buses following the clearance of the disturbance

$$\text{TPSI} = \frac{\sum_{i=1}^{N}\sum_{t=T_c}^{T}(|P_i^t - P_i^0|/P_i^0)}{N \times (T - T_c)} \tag{3}$$

where N is the total number of buses in the system, T_c is the fault clearing time, P_i^0 is power magnitude of bus i before the fault occurrence, and P_i^t is the power magnitude of bus i at time t obtained from time-domain simulation.

Here, the first objective is minimization of the VSI, f_1, and second objective is minimization of the TPSI, f_2, calculated by (1) and (3), respectively. It should be noted that (1) and (3) cannot be explicitly calculated and they need a time-domain simulation to achieve the post-disturbance voltage and power trajectories.

2) Constraints: In this study, the constraints of the MOP model are represented as the steady-state constraints and dynamic constraints. The steady-state constraints consist of power flow balance and steady-state operational limits for pre-contingency state

$$\begin{cases} P_G - P_L - P(V,\theta) = 0 \\ Q_G - Q_L - Q(V,\theta) = 0 \end{cases} \tag{4}$$

$$\begin{cases} S(V,\theta) \le S^{\max} \\ V^{\min} \le V \le V^{\max} \\ P_G^{\min} \le P_G \le P_G^{\max} \\ Q_G^{\min} \le Q_G \le Q_G^{\max} \\ Q_{STAT}^{\min} \le Q_{STAT} \le Q_{STAT}^{\max} \end{cases} \tag{5}$$

where (4) represents the active and reactive power balance for each bus, and P_G and Q_G represent the active and reactive power generations, P_L and Q_G represent the active and reactive power loads, P and Q represent the power flow equations, V is the voltage bus, and θ is the voltage angle. (5) represents the operational limits on line flow, steady-state voltage magnitude, generators output capacity (including conventional generators and DFIG), and the STATCOM reactive power capacity.

Also, adding dynamic constraints such as the rotor angle stability constraint is important for the proposed optimization model to avoid the voltage instability. Generally, the rotor angle stability is tested by examining the rotor angle deviation against a certain threshold [16]. In this paper, the following constraint is included to ensure the rotor angle stability for any contingency

$$[\max(\Delta\delta_{ij}^T)] \le \beta \tag{6}$$

where $[\max(\Delta\delta_{ij}^T)]$ represents the the maximum rotor angle deviation between any two generators during the transient period T and β is the threshold which can be set to π for the extreme case [16].

B. Solution Method

1) Pareto Optimality: The two-objective optimization problem presented in Section III-A requires to be solved. Based on the priority of the objective functions, a MOP has multiple solutions, which can form a Pareto-optimal set (set of all the Pareto optimal solutions) [16], where decision-maker may select any of them depending on practical needs. Given the control variables vector $\boldsymbol{X} = [x_1, x_2, \dots x_n]$, a vector $\boldsymbol{X^*} = [x_1^* \; x_2^* \; \dots \; x_n^*]$ is the Pareto-optimal set, or the non-dominated solutions, if any point in $\boldsymbol{X}$ satisfies $f_j(\boldsymbol{X}) \le f_j(\boldsymbol{X^*})$ for all $j = 1, 2, \dots, m$ (f_j denotes to objective function, while m is the number of the objective function).

2) Normalized Simulated Annealing (NSA): When dealing with a MOP, stochastic methods are superior to classical strategies because they can simultaneously find Pareto-optimal solutions [12]. The stochastic NSA algorithm has the ability to search in very large spaces of candidate solutions and avoid becoming trapped in local minima, with lower computational time compared to other stochastic methods. This technique was early introduced by Kirkpatrick et al. for finding a global minimum of an optimization function [13]. It is based on an analogy between the way in which a metal cools and freezes into a minimum energy crystalline structure (annealing process). The algorithm employs a random search, where random moves are accepted with a probability function $pr = exp(-\Delta f/Tf)$, where Δf is increasing in f and Tf is the system temperature during the cooling process [14].

Since two objective functions presented in Section III-A must be prioritized according to the power system operator's needs, a cooling schedule, taking into account the prioritization of the these objective functions, is proposed by assigning a different initial temperature for each objective, i.e., Tf_1 and Tf_2. If the initial temperature is given to an objective in a high order (i.e. high priority), the probability of accepting a solution is higher than that objective with lower initial temperature (i.e. less given priority). Moreover, since these two objective functions are not coherent, these should be normalized by dividing their initial values in order to make them comparable to each other. The rest of the optimization parameters are the number of iterations, max$iter$, upper and lower bounds of the variables, $\boldsymbol{X}^{max}$ and $\boldsymbol{X}^{min}$, which determine the search area and the rate of the temperatures change r_b, which is positive and less than 1. The detailed steps of the NSA algorithm are shown in Table I.

C. Tuning the FLC Model Using NSA

The FLC used in this paper is based for two inputs; i.e., the two initial temperatures Tf_1 and Tf_2 assigned to two objectives f_1 and f_2, respectively. The output of the FLC system are defined with two optimal control variables, i.e. Q_{RSC}^* and Q_{STAT}^*, which are obtained by the NSA optimization algorithm in form of Pareto-optimal solutions. Each of the two input and two output variables is divided into the three fuzzy subsets corresponding to meanings of "low" (L), "medium" (M), and "high" (H). All fuzzy subsets are modeled with sigmoid membership functions [17]. Fuzzy input subsets and fuzzy output subsets are generated by selecting the parameters m and σ, as given in Table II and shown in Fig. 2.

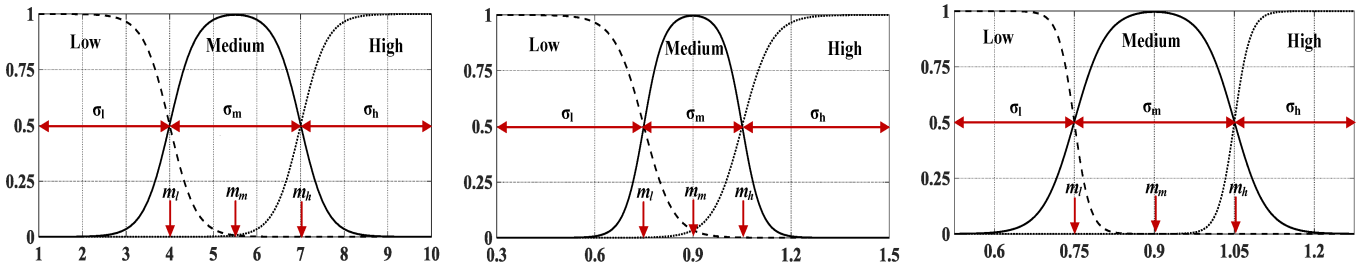

Fig. 2. Fuzzy membership functions. (a) Fuzzy input subsets of the Tf_1 and Tf_2. (b) Fuzzy output subset of the Q^*_{RSC}. (c) Fuzzy output subset of the Q^*_{STAT}.

TABLE I
NORMALIZED SIMULATED ANNEALING (NSA) ALGORITHM

Define an initial Tf_j for each objective and **Set** $iter = 1$
Create randomly an initial solution $\boldsymbol{X} = [x_1, x_2, \dots x_n]$ for $\boldsymbol{X^{min}} \le \boldsymbol{X} \le \boldsymbol{X^{max}}$
Calculate objective values of $\{f_1(\boldsymbol{X}), f_2(\boldsymbol{X}), \dots, f_m(\boldsymbol{X})\}$
Produce new random solutions using the nonuniform mutation operator
  for $i = 1$ to n
Create a uniformly distributed random number $0 < \boldsymbol{rand_i} < 1$
Generate a random binary number bin
    if $bin = 1$ **then**
    $x_i^{new} = x_i^{iter} + (x_i^{max} - x_i^{iter}) \cdot rand_i \cdot exp(-iter/\text{max}iter)$
    else
    $x_i^{new} = x_i^{iter} + (x_i^{iter} - x_i^{min}) \cdot rand_i \cdot exp(-iter/\text{max}iter)$
    end if
  end for
Normalized the objective functions for obtained solutions
  $f_j^{norm}(\boldsymbol{X}) = f_j(\boldsymbol{X}^{new})/f_j(\boldsymbol{X}^{iter})$
    for $j = 1, 2, \dots, m$
Calculate the probabilities of the new solutions
  $\Delta f_j = f_j^{norm}(x_1^{new}, \dots, x_n^{new}) - f_j^{norm}(x_1^{iter}, \dots, x_n^{iter})$
    for $j = 1, 2, \dots, m$
    if $\Delta f_j \ge 0$ **then**
      $pr_j = exp(-\Delta f_j / Tf_j)$ **else** $pr_j = 1$
    end if
Produce m random numbers $\boldsymbol{rand_j}$
    if $\forall rand_j < pr_j$ for $j = 1, 2, \dots, m$ **then**
      $x_i^{iter+1} = x_i^{new}$ **else** $x_i^{iter+1} = x_i^{iter}$
    end if
Set $Tf_j = r_b Tf_j$ and $iter = iter + 1$
    if $iter <$ max$iter$ **then goto** step 3
      else $\boldsymbol{X^*} = \boldsymbol{X}^{\text{max}iter}$
  The Pareto-optimal solutions are $\boldsymbol{X^*} = [x_1^*, x_2^*, \dots, x_n^*]$
    end if
Exit

In this paper, the changes made to parameter of m are only taken into consideration for tuning the output fuzzy subsets model. As shown in Table III, the continuous variables y_1 and y_2 indicate adjustable parameters the output fuzzy subsets. The effects of making changes on output fuzzy membership functions have been simultaneously studied by using the NSA algorithm. This optimization approach is presented for tuning the fuzzy model (Fig. 2(b) and (c)) by determining the suitable value of y_1 and y_2 and also creating the fuzzy rules (or Pareto-optimal classification rules) using the obtained Pareto-optimal solutions. The reason for selecting the NSA-based approach for tuning the FLC is that the proposed combinatory DFIG-based WT and the STATCOM is a high-dimensional multivariate time-varying system and the derivation of rules from the simple

TABLE II
PARAMETERS USED TO GENERATE INITIAL SIGMOID MEMBERSHIP FUNCTIONS FOR INPUT AND OUTPUT VARIABLES

Variables	Variation range	Low subset m_l	Low subset σ_l	Mid subset m_m	Mid subset σ_m	High subset m_h	High subset σ_h
$Tf_{1,2,3}$	[1, 2, …, 10]	4	3	5.5	3	7	3
Q^*_{RSC}	(0.3 1.5)	0.75	0.45	0.9	0.3	1.05	0.45
Q^*_{STAT}	(0.5 1.275)	0.75	0.225	0.9	0.3	1.05	0.225

TABLE III
PARAMETERS USED TO GENERATE TUNABLE SIGMOID MEMBERSHIP FUNCTIONS FOR OUTPUT VARIABLES

Variables	Low subset m_l	Low subset σ_l	Mid subset m_m	Mid subset σ_m	High subset m_h	High subset σ_h
Q^*_{RSC}	y_1	0.45	y_1+0.15	0.3	y_1+0.3	0.45
Q^*_{STAT}	y_2	0.225	y_2+0.15	0.3	y_2+0.3	0.225

fuzzy reasoning is entirely complicated. The procedure of fuzzy model and fuzzy rules tuning is designed using the following five steps:

*1) **Initialization**:* There are two control variables (Q_{RSC} and Q_{STAT}) for the NSA algorithm and also two adjustable parameters (y_1 and y_2) for the FLC model, which can be formulated as the vector $\boldsymbol{X} = [Q_{RSC}\ Q_{STAT}]^T$ and the vector $\boldsymbol{Y} = [y_1\ y_2]^T$. The upper and lower bounds, $\boldsymbol{X}^{max}$ and $\boldsymbol{X}^{min}$ of the control parameters and the upper and lower bounds, $\boldsymbol{Y}^{max}$ and $\boldsymbol{Y}^{min}$ of the fuzzy variables must be specified to determine the range of the searching apace, given by

$$\begin{cases} 0.3 \le Q_{RSC} \le 1.5\ MVar, \\ 0.5 \le Q_{STAT} \le 1.27\ MVar, \\ 0.69 \le y_1 \le 0.81,\ 0.69 \le y_2 \le 0.81, \end{cases} \tag{7}$$

In this paper, the limitations of the control variables for the optimization problem are determined with two principles; 1) RSC of the DFIG should have the minimum contribution of 20% (0.3 MVar from 1.5 MVar) for fault ride-through requirement during the fault; and 2) STATCOM must provide the minimum value of steady-state reactive power 0.5 MVar and the maximum 85% of its total capacity (i.e., 1.27 MVar from 1.5 MVar) for safe operation during the fault. Hence, the upper and lower bounds for optimization process are: $\boldsymbol{X}^{min}$=[0.3 0.5]^T, $\boldsymbol{X}^{max}$=[1.5 1.27]^T, $\boldsymbol{Y}^{min}$=[0.69 0.69]^T, and $\boldsymbol{Y}^{max}$=[0.81 0.81]^T.

TABLE IV
FUZZY RULES GENERATED BY NSA

Rule No.		Fuzzy Input $Tf_1 - Tf_2$		Fuzzy Output $Q^*_{RSC} - Q^*_{STAT}$
1	**IF**	$High - High$	**THEN**	$Medi - High$
2	**IF**	$High - Medi$	**THEN**	$Medi - High$
3	**IF**	$High - Low$	**THEN**	$High - High$
4	**IF**	$Medi - High$	**THEN**	$Low - High$
5	**IF**	$Medi - Low$	**THEN**	$High - High$
6	**IF**	$Low - High$	**THEN**	$Low - Low$
7	**IF**	$Low - Medi$	**THEN**	$Low - Low$

As an arbitrary choice, each objective of the MOP model $f_1(Q_{RSC}, Q_{STAT})$ and $f_2(Q_{RSC}, Q_{STAT})$, where f_1 and f_2 denote to VSI and TPSI, respectively, is assigned an initial temperature of Tf_1 and Tf_2 based on their priority selection, i.e., low ($Tf_{1,2}$=1), medium ($Tf_{1,2}$ =5), and high ($Tf_{1,2}$ =10). As mentioned in Section III-C, two initial temperatures Tf_1 and Tf_2 are considered for the input fuzzy system, which are divided into the three fuzzy subsets. For three input fuzzy subsets, there are 7 possible cases that are needed to convert into equivalent fuzzy rules after 7 optimization round process, as shown in Table IV.

*2) **Selecting optimization round from Table IV**:* At the first round of the optimization, the initial temperatures of Tf_1=10 and Tf_2=10 for two objectives is selected with the corresponding initial fuzzy input $High - High$ as the rule number 1, while it is shifted to the next rule at the end of each optimization round, until reaching the rule number 7 (i.e., updating the fuzzy rules). Moreover, the output fuzzy subsets (Fig. 2(b) and (c)) are generated using initial values of y_1=y_2= 0.75 at the first round of the optimization, and are then regenerated simultaneously at the next round of the optimization based on the updated variables of y_1 and y_2 (i.e., updating the fuzzy model).

In the proposed NSA algorithm, 100 iterations (max$iter$ = 100) is considered for each round of the optimization. Set $iter = 1$ and start the optimization process with step 3.

*3) **Generating new random solution**:* Create randomly an initial solution $\boldsymbol{X}^{iter} = [Q^{iter}_{RSC}\ Q^{iter}_{STAT}]^T$ inside the predefined searching space. To produce new control variables $\boldsymbol{X}^{new} = [Q^{new}_{RSC}\ Q^{new}_{STAT}]^T$ based on the current solutions, an update for each parameter is calculated at each iteration. If random binary $bin = 1$, then

$$\boldsymbol{X}^{new} = \boldsymbol{X}^{iter} + (\boldsymbol{X}^{max} - \boldsymbol{X}^{iter}) \cdot rand(0,1) \cdot exp(-iter/\text{max}iter) \tag{8}$$

else

$$\boldsymbol{X}^{new} = \boldsymbol{X}^{iter} + (\boldsymbol{X}^{iter} - \boldsymbol{X}^{min}) \cdot rand(0,1) \cdot exp(-iter/\text{max}iter) \tag{9}$$

Also, new adjustable parameters $\boldsymbol{Y}^{new} = [y_1^{new}, y_2^{new}]$ are computed based on a random value between [-0.5, 0.5] and the current temperature of each objective by

$$\boldsymbol{Y}^{new} = \boldsymbol{Y}^{iter} + rand(-0.5, 0.5) \cdot [(Tf_1^{iter} + Tf_2^{iter})/(Tf_1^{initial} + Tf_2^{initial})] \tag{10}$$

As the temperature decreases, changes in parameters of y_1 and y_2 decreases proportional to the temperature decrease.

*4) **Selecting new solution for next iteration**:* The probability of selecting the new control variables $\boldsymbol{X}^{new}$ for f_1 and f_2 are obtained after normalizing the objective functions, as follows

$$\begin{cases} \Delta f_1 = f_1^{norm}(Q^{new}_{RSC}, Q^{new}_{STAT}) - f_1^{norm}(Q^{iter}_{RSC}\ Q^{iter}_{STAT}) \\ \Delta f_2 = f_2^{norm}(Q^{new}_{RSC}, Q^{new}_{STAT}) - f_2^{norm}(Q^{iter}_{RSC}\ Q^{iter}_{STAT}) \end{cases} \tag{11}$$

$$pr_j = \begin{cases} exp(-\Delta f_j / Tf_j^{iter}), & \text{if } \Delta f_j \geq 0 \\ 1, & \text{if } \Delta f_j < 0 \end{cases} \tag{12}$$

for $j = 1$ and $j = 2$. If $(pr_1 > r_1)$ and $(pr_2 > r_2)$

$$\begin{cases} \textbf{Then} & [Q^{iter+1}_{RSC}\ Q^{iter+1}_{STAT}]^T = [Q^{new}_{RSC}\ Q^{new}_{STAT}]^T \\ \textbf{Else} & [Q^{iter+1}_{RSC}\ Q^{iter+1}_{STAT}]^T = [Q^{iter}_{RSC}\ Q^{iter}_{STAT}]^T \end{cases} \tag{13}$$

where r_1 and r_2 are uniformly distributed random numbers in [0, 1]. The adjustable parameters of $\boldsymbol{Y}$ for the next iteration of the optimization can be achieved as

If $Q^{iter+1}_{RSC} \in [0.45, 0.9]$ and $Q^{iter+1}_{STAT} \in [0.6, 0.9]$,

$$\begin{cases} \textbf{Then} & [y_1^{iter+1}\ y_2^{iter+1}]^T = [y_1^{new}\ y_2^{new}]^T \\ \textbf{Else} & [y_1^{iter+1}\ y_2^{iter+1}]^T = [y_1^{iter}\ y_2^{iter}]^T \end{cases} \tag{14}$$

*5) **Updating fuzzy model and fuzzy rules**:* In this step, the Pareto-optimal solutions for control variables $\boldsymbol{X}$ and optimal adjustable parameters $\boldsymbol{Y}$ will be updated after each round (there is 7 round optimization).

Set $Tf_1^{iter+1} = r_b Tf_1^{iter}$, $Tf_2^{iter+1} = r_b Tf_2^{iter}$, and $iter = iter + 1$. If $iter <$ max$iter$, then go to step 3 to keep iterating. Otherwise, the search process will be terminated with $[Q^*_{RSC}\ Q^*_{STAT}]^T = [Q^{\text{max}iter}_{RSC}\ Q^{\text{max}iter}_{STAT}]^T$ and $[y_1\ y_2]^T = [y_1^{\text{max}iter}\ y_2^{\text{max}iter}]^T$.

The Pareto-optimal solutions X^* obtained at each round of optimization process is used to update fuzzy rules, as presented in Table IV. Also, the obtained Y values is used to update the output fuzzy subset configurations, as shown in Fig. 2(b), (c), based on the tunable fuzzy model given in Table II. If the round number of the optimization process is 7, then stop optimization process(tuning the fuzzy model and fuzzy rules are completed); otherwise, go to step 2.

III. COMPUTER SIMULATION STUDY

In previous sections, the mathematical formulations are derived in order to find the optimal values of the compensating reactive power for both the RSC of the DFIG and the STATCOM controllers. It was achieved via the FLC, which is properly tuned using the NSA algorithm. In this section, the simulations in MATLAB/SIMULINK are presented to validate the effectiveness of the proposed control approach.

A. Power System Case Study

The original four-machine 12-bus benchmark power system in [18] was used as a platform system to study the flexible ac transmission system (FACTS) device applications for the transient stability analysis. In this paper, the single-line diagram of the four-machine 12-bus power system is modified by placing

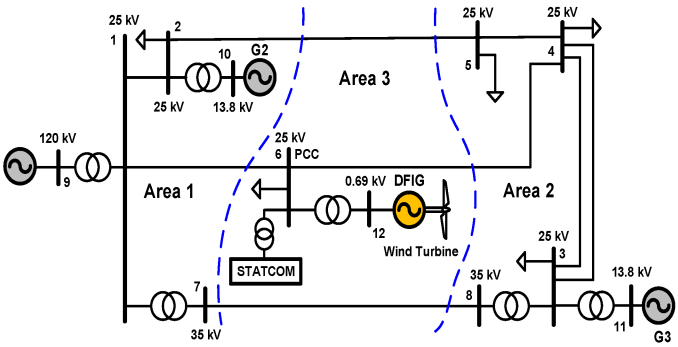

Fig. 3. Single-line diagram of the multi-machine benchmark power system including a wind turbine and a STATCOM connected to the PCC.

a WT and a STATCOM at bus 6 (PCC), as shown in Fig. 3. The system covers three geographical areas; area 1 represents the main generation area with two hydro power generation G1 and G2; area 2 represents the main load center with a hydro power generation G3; and area 3 represents the proposed combination of the 1.5 MW DFIG-based WT and the 1.5 MVar STATCOM. For dynamic studies, in this paper, the conventional generators of G1, G2, and G3 are modeled in detail, in which the exciter and turbine governor dynamic models are taken into account. The detailed dynamic specifications of the conventional generators, as well as 12-bus system parameters are given in [18].

A 1.5-MW DFIG driven by a WT, with the wind speed 12 m/s and rotor speed 1.2 p.u, is connected to a power grid through a 0.69/25 kV transformer. The DFIG system is a wound-rotor induction generator, in which the stator winding is directly connected to the three-phase grid and the rotor winding is fed through the three-phase back-to-back IGBT based PWM converters. The back-to-back converters consist of three parts: a RSC, a GSC, and a dc-link capacitor placed between the two converters. A STATCOM, which is connected to the PCC via a 13.8/25 kV transformer, is modeled as a gate-turn-off thyristor (GTO) PWM converter with a dc-link capacitor [4].

The detailed dynamic models of the DFIG and the STATCOM, as well as the control scheme for both of them are well documented in the literature [1], [2], [4], as employed in this section for the MATLAB simulation. The vector control strategy is used for the active and reactive power control of the DFIG and the STATCOM. Control of the DFIG is achieved by control of the RSC an the GSC. The RSC is used to control both the stator active and reactive powers independently. The reactive power control provided by the RSC can be used during the fault to keep the stator voltage within the desired range, when the DFIG connected into a weak power system with inadequate local reactive compensation. The GSC is used to maintain the dc-link voltage at a constant level. In this paper, the GSC control scheme is also designed to set its reactive current reference at a zero value. This setting is reasonable since the DFIG converters are rated for only $25\% - 30\%$ of the generator rating, which are primarily used for transferring the active and reactive power from the rotor to the grid. A STATCOM is used to provide a rapid and controllable reactive power compensation during the fault to help with the uninterrupted operation of the WT under disturbance. In this paper, the STATCOM provides the steady-state fixed reactive power of 0.5 MVar for voltage support as well as the desired amount of reactive power during the fault for the transient reactive power support.

TABLE V
PARETO OPTIMALITY RESULTS USING NSA ALGORITHM

Case No.	Priority $Tf_1 - Tf_2$	Q^*_{RSC} (MVar)	Q^*_{STAT} (MVar)	VSI	$TPSI$
1	$10-10$	1.02	1.06	0.236	0.336
2	$10-5$	1.04	1.12	0.233	0.396
3	$10-1$	1.42	1.15	0.227	0.486
4	$5-10$	0.62	1.18	0.258	0.186
5	$5-1$	1.13	1.08	0.230	0.408
6	$1-10$	0.43	0.76	0.375	0.144
7	$1-5$	0.56	0.86	0.298	0.168

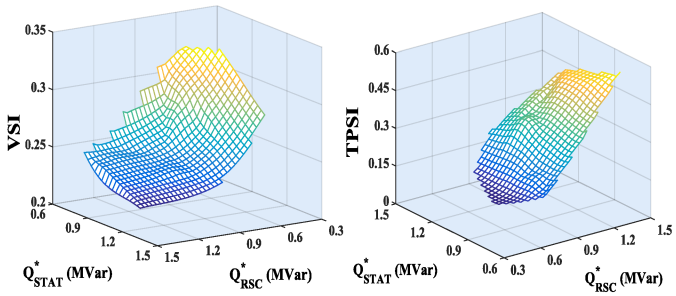

Fig. 4. Three dimensional representations of control variables versus objective function.

A three-phase symmetrical grid fault is considered, since the fault ride-through capability of the regional grid codes mostly refer to this type of fault. Thus, a three-phase fault is applied to the bus 1 end of line $1-6$ at $t = 40$ s ($T_s = 40$) and is cleared after 150 ms ($T_c = 40.15$), resulting in a 40% depth of voltage dip at the PCC. The offline tuning of the FLC model, via proposed NSA algorithm, were accomplished by means of MATLAB programming.

B. Validation of the NSA Algorithm

Table V shows 7 optimization round process results of the tuning algorithm due to the temperature changes of the two objectives based on priority selection (i.e., low (1), medium (5), and high (10)). The corresponding results are used to plot the variation of the objective functions, VSI and $TPSI$ versus the control variables Q^*_{RSC} and Q^*_{STAT}, shown in Fig. 4, which are interpolated for better visualization. It can be seen that increasing the amount of Q^*_{DFIG} and Q^*_{STAT} is needed to minimize VSI. However, the large value Q^*_{RSC} increases the $TPSI$.

Fig. 5 schematically depicts the progression of the control variables and objective functions of the optimization problem after 100 iterations, considering the first objective (VSI) as a high priority and the second objective ($TPSI$) as a low priority. The results clearly show that the reactive power commands and objective functions rapidly converge in an optimal point during the cooling (annealing) process.

For comparative purposes, the optimization process is verified by another algorithm, i.e., the non-dominant sorting GA version II (NSGA-II) [19]. The NSGA-II approximates the entire Pareto front, and no modification could be made to locate only the optimal solutions corresponding to the multi-objectives problems. The best parameters of NSGA-II optimization for the proposed problem are achieved with a population size of 60, a crossover probability of 0.85, and a mutation probability

978-1-4673-8672-2/15/$31.00 © 2016 IEEE

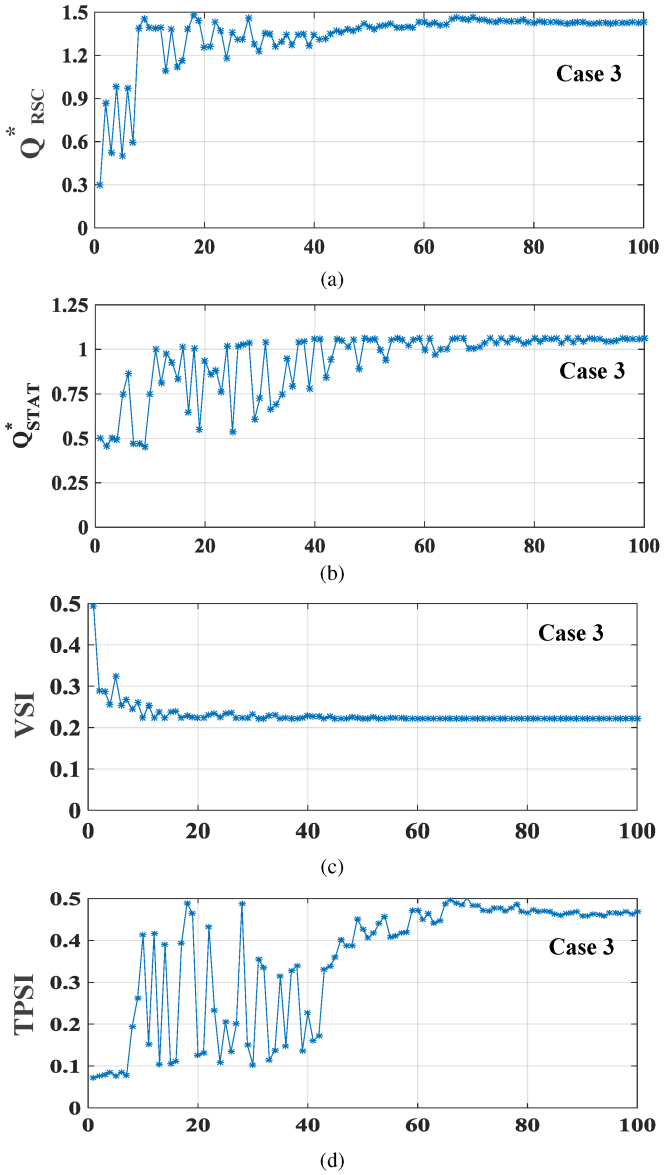

Fig. 5. NSA-based optimization progress of the reactive power commands (control variables) and two objectives for the case 3; x-axis denotes to the number of iteration.

of 0.15, resulting with the final Pareto-optimal solutions after 100 iterations. Table VI presents the total computational times, using a PC with an Intel core i7-4770/3.5-GHz, the average errors, and the error variances that were produced by the two methods.

Compared to the NSGA-II algorithm, the proposed method exhibits considerably lower computational times, which is reliable for online application, where the control system needs to act in a very short period of time. The Fig. 6 shows the Pareto front (set of all the Pareto optimal objective values), which is produced by the tradeoff among the 7 sets of mutually contradicting control variables. These results are compared with 11 optimal objective values obtained by the NSGA-II algorithm.

All these solutions lying on the Pareto front are non-dominated solutions, so that they can be selected with the individual decision makers based on his/her own preference. For some regional grid codes, such as Australia, Denmark and Germany, which supporting the reactive power under fault

TABLE VI
COMPARISON OF THE NSA PERFORMANCE WITH NSGA-II

Optimization Algorithm	Number of iterations(s)	iteration time(s)	Total time(s)	Average error	Error Variance
NSA	100	0.41	41	0.605	0.144
NSGA-II	100	1.55	155	0.121	0.017

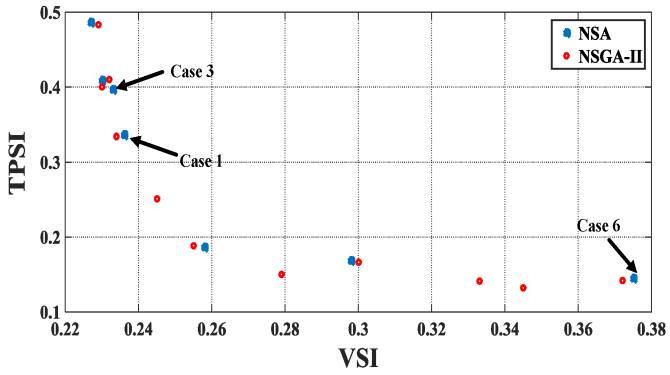

Fig. 6. Pareto front that was obtained with NSGA-II and NSA algorithm.

conditions has highest priority [1], the cases of 2, 3 and 5 in Table V can be suitable choices. On the contrary, for some regional grid codes, such as Ireland, Spain and the UK, where supplying the active power to the grid during and even after the faults has higher priority compared with reactive power [1], more contribution of the STATCOM should be taken into consideration in order to compensate required reactive power for the stability improvement. Thus, in these grid reginal grid codes, the cases the cases of 4, 6 and 7 can be proper candidates. The case 1 could be a proper selection, when supplying the active and reactive power have the same importance.

It should be also mentioned that the concept of the proposed reactive control strategy during the fault is applicable to various sizes of the WT and STATCOM. The only variation would be in the upper and lower bounds, $\mathbf{X}^{max}$ and $\mathbf{X}^{min}$ of the control variables in order to determine the searching space for the proposed optimization problem.

C. Simulation Case Studies

For validation purposes, the dynamic performance of the combinatorial WT and the STATCOM, were reinforced with the proposed control approach in case numbers of 1, 3, and 6; compared with the case without the proposed control system, where all control parameters under fault condition were the same with the steady-state condition.

Case No.1 from Table V: in case number 1, the proposed control system was optimally designed to minimize both objective functions by assigning the highest priority ($Tf_1 = 10$ and $Tf_2 = 10$) to the VSI and $TPSI$. In this case, both the RSC and the STATCOM have almost a same contribution for generating the reactive powers during the faults in order to improve transient behavior of the voltage and power at the PCC during and after clearing the fault. Accordingly, reactive power commands of the RSC and the STATCOM were quickly changed to high values of Q^*_{RSC} =1.02 MVar and Q^*_{STAT} =1.06 MVar during the fault, as shown in Figs. 7(c) and (d). In this case, the depth of the voltage dip is about 24%,

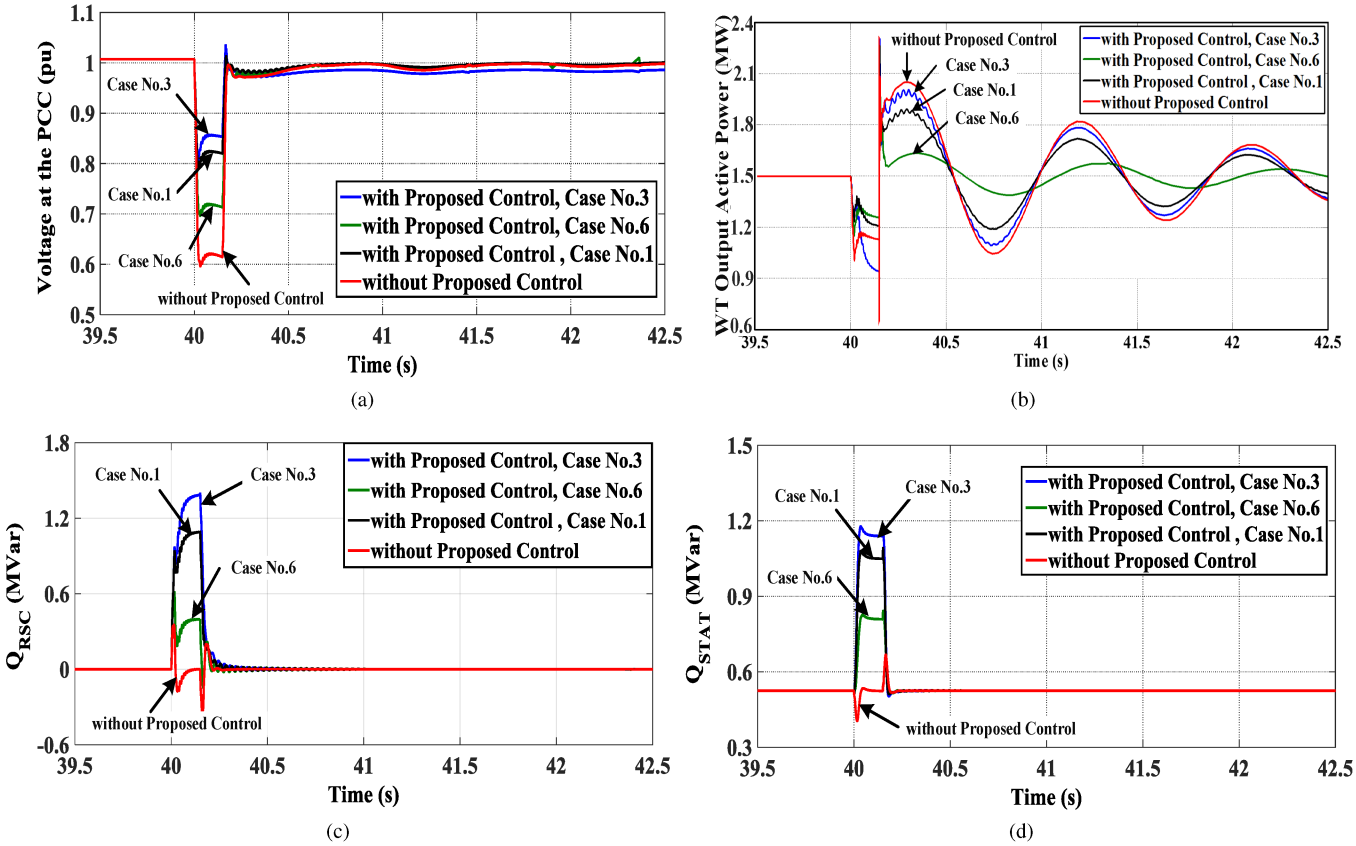

Fig. 7. Dynamic response of the 12-bus system with and without proposed control system considering case 1, case 3, and case 6. (a) Voltage at PCC. (b) Output active power at the PCC. (c) Output reactive power of WT. (d) Output reactive power of STATCOM.

as shown in Fig. 8. The post-fault active power oscillations in case number 1 are damped more rapidly than in case number 3, but this is still less rapidly than in case number 3 (see Fig. 7(b)). These results confirm that the proposed control system enhances the LVRT capability of the WT and power oscillation damping of the system during transient conditions.

Case No.3 from Table V: in case number 3, the proposed control system was optimally designed to minimize the voltage deviations at the PCC during the fault by assigning the highest priority to the objective VSI. Thus, more contribution of the RSC and STATCOM should be taken into consideration, in order to compensate required reactive power for voltage stability improvement of the weak power system. As shown in Fig. 7(a), the proposed control approach significantly reduces the magnitude of voltage sag to around 15%. Accordingly, reactive power commands of the RSC and the STATCOM were quickly changed to high values of Q^*_{DFIG} =1.42 MVar and Q^*_{STAT} =1.15 MVar during the fault, as shown in Fig. 7(c) and Fig. 7(d). After the fault clearing at t = 40.15 s, reactive power values return to their predefined values in the steady-state condition. As it can be noticed in Fig. 7(b), the proposed control system in case 3 is not able to reduce the active power oscillations at the PCC due to lower priority of $TPSI$ compared to VSI.

Case No.6 from Table V: in case number 6, the proposed control system was optimally designed to enhance power oscillation damping in power system after clearing the fault, by assigning the highest priority to the objective $TPSI$. In Fig. 7(a), it can be observed that this case is unable to improve the voltage deviation at the PCC due to lower priority VSI compared to $TPSI$, where magnitude of voltage sag reaches approximately 30%. Accordingly, the reactive power commands of the RSC and the STATCOM were both set at low values of Q^*_{DFIG} = 0.43 MVar and Q^*_{STAT} = 0.76 MVar during the fault, as shown in Fig. 7(c) and Fig. 7(d). The post-fault active power oscillations in case 3 is damped more rapidly than other cases (Fig. 7(b)).

IV. Conclusion

This paper presents a computational intelligence technique in order to design an external interface controller for the coordinated reactive power control between the WT and the STATCOM, during the faults. The overall problem is formulated as a multiobjective optimization model, minimizing two conflicting objectives, and solved by stochastic NSA algorithm. This approach provides a Pareto front for decision makers to determine the optimal tradeoff between reducing the voltage deviations during and after the fault and damping the active power oscillations during the recovery period. Compared to the NSGA-II method, it is clearly confirmed the NSA exhibits considerably lower computational times (NSA is around 3.7 times faster than NSGA-II). The transient active power performance of the system after the fault clearing time is quantified by the so-called TPSI. For online applications, the optimal commanded values of the compensating reactive power for both RSC of the DFIG and the STATCOM controllers have been

TABLE VII
PARAMETERS OF THE 1.5-MW DFIG

Parameters	Value	Parameters	Value
Rated power	1.5 MW	Stator inductance	0.171 pu
Rated voltage	0.69 kV	Rotor inductance	0.156 pu
Rated frequency	60 Hz	Magnetizing inductance	2.9 pu
Rated wind speed	12 m/s	Rotational inertia	5.04 s
Stator resistance	0.007 pu	dc-link voltage	1.2 kV
Rotor resistance	0.005 pu	dc bus capacitor	50 mF

achieved via an FLC which is properly tuned using the NSA algorithm. Simulation results have shown that the proposed control approach can successfully improve the LVRT capability of the WT in the weak grid-connected mode. Moreover, it can operate as an external damping controller for the WT, and therefore, improve the post-fault power oscillation damping of system.

APPENDIX A

Table VII shows the 1.5 MW DFIG parameters, which are used in the simulation results.

REFERENCES

[1] W. Qiao, G. K. Venayagamoorthy, R. G. Arnaltes, "Real-time implementation of a STATCOM on a wind farm equipped with doubly fed induction generators," *IEEE Trans. Energy Convers*., vol. 45, no. 1, pp. 98−107, 2009.

[2] T. Tang, J. Ping, H. Hiabo, Q. Chuan, W. Feng, "Optimized control of DFIG-based wind generation using sensitivity analysis and particle swarm optimization," *IEEE Trans. Smart Grid*., vol. 4, no. 1, pp. 509−520, 2013.

[3] F. K. A. Lima, A. Luna, P. Rodriguez, E. H. Watanabe, F. Blaabjerg, "Rotor voltage dynamics in the doubly fed induction generator during grid faults," *IEEE Trans. Power Electron*., vol. 25, no. 1, pp. 118−130, 2010.

[4] W. Qiao, R. G. Harley, G. K. Venayagamoorthy, "Coordinated reactive power control of a large wind farm and a STATCOM using heuristic dynamic programming," *IEEE Trans. Energy Convers*., vol. 24, no. 2, pp. 493−503, 2009.

[5] H. Gaztanaga, I. Etxeberria-Otadui, D. Ocnasu, S. Bacha, "Real-time analysis of the transient response improvement of fixed-speed wind farms by using a reduced-scale STATCOM prototype," *IEEE Trans. Power Syst*., vol. 22, no. 2, pp. 658−666, 2007.

[6] Y. Mishra, S. Mishra, and F. Li, "Coordinated tuning of DFIG-based wind turbines and batteries using bacteria foraging technique for maintaining constant grid power output," *IEEE Trans. Power Syst. J*.., vol. 6, no. 1, pp. 1626, Mar. 2012.

[7] F. M. Gonzalez-Longatt, P. Wall, P. Regulski, and V. Terzija, "Optimal electric network design for a large offshore wind farm based on a modified genetic algorithm approach," *IEEE Trans. Power Syst. J*.., vol. 6, no. 1, pp. 164172, Mar. 2012.

[8] F. Wu, X. P. Zhang, K. Godferey, P. Ju, "Small signal stability analysis and optimal control of a wind turbine with doubly fed induction generator," *IET Gener. Transm. Distrib*., vol. 1, no. 5, pp. 751−760, 2007.

[9] T. D. Vrionis, X. I. Koutiva, N. A. Vovos, "A genetic algorithm-based low voltage ride-through control strategy for Grid Connected Doubly Fed Induction Wind Generators," *IEEE Trans. Power Syst*., vol. 29, no. 3, pp. 1325−1334, 2014.

[10] G. K. Venayagamoorthy, "Dynamic, stochastic, computational, and scalable technologies for smart grids," *IEEE Comput. Intell. Mag*., vol. 6, no. 3, pp. 22−35, 2011.

[11] Y. Tang, H. He, Z. Ni, J. Wen, X. Sui, "Reactive power control of grid-connected wind farm based on adaptive dynamic programming," *Neurocomputing*., vol. 78, no. 1, pp. 3−13, 2012.

[12] E. Aggelogiannaki and H. Sarimveis, "A simulated annealing algorithm for prioritized multiobjective optimization implementation in an adaptive model predictive control configuration," *IEEE Trans. Systems, Man, and Cybernetics, Part B: Cybernetics*., vol. 37, no. 4, pp. 902−915, 2007.

[13] S. Kirkpatrick, C. D. Gelatt, M. P. Vecchi, "Optimization by simulated annealing," *Science*., vol. 220, pp. 671−680, 1983.

[14] H. Heydari and A. H. Moghadasi, "Optimization scheme in combinatorial UPQC and SFCL using normalized simulated annealing," *IEEE Trans. Power. Del*., vol. 26, no. 3, pp. 1489−1498, 2011.

[15] M. Mohseni and S. M. Islam, "Review of international grid codes for wind power integration: Diversity, technology and a case for global standard," *Renew. Sustain. Energy Rev*., vol. 16, no. 6, pp. 3876−3890, 2012.

[16] Y. Xu, Z. Y. Dong, K. Meng, W. F. Yao, R. Zhang, K. P. Wong, "Multi-objective dynamic VAR planning against short-term voltage instability using a decomposition-based evolutionary algorithm," *IEEE Trans. Power Syst*., vol. 29, no. 6, pp. 2118−2822, Nov. 2014.

[17] I. M. Garibaldi and E. C. Ifeachor, "Application of simulated annealing fuzzy model tuning to umbilical cord acid-base interpretation," *IEEE Trans. Fuzzy Syst*., vol. 7, no. 1, pp. 72−84, 1999.

[18] S. Jiang, U. D. Annakkage, and A. M. Gole, "A platform for validation of FACTS models," *IEEE Trans. Power. Del*., vol. 21, no. 1, pp. 484−491, Jan. 2006.